

# A slip tendency analysis to test mechanical and structural control on aftershock rupture planes

Cristiano Collettini\*, Fabio Trippetta

*Geologia Strutturale e Geofisica Dipartimento di Scienze della Terra Università degli studi di Perugia, Italy*

Received 26 October 2006; received in revised form 6 December 2006; accepted 2 January 2007

Available online 9 January 2007

Editor: R.W. Carlson

## Abstract

Large portions of intraplate regions are characterised by relatively uniform stress fields with moderate to large main shock fault-ruptures nucleating on planes successfully predicted by 2D frictional fault reactivation theory. Here we use a slip tendency analysis, based on the notion that slip on a fault is controlled by the ratio of shear stress to normal stress acting on the plane of weakness, to test whether aftershock sequences are also governed by fault reactivation theory within the regional stress field. We observe that aftershocks for two well-documented seismic sequences occurring in extensional and compressional environments, the 1997  $M_w=6.0$  Colfiorito sequence (Central Italy) and the 1999  $M_w=7.5$  Chi-Chi sequence (Taiwan), respectively, nucleate on planes favourably oriented for frictional fault reactivation. In particular, 89% of 329 and 81% of 121 events for the Colfiorito and Chi-Chi sequences respectively, are the result of fault reactivation processes on geological structures that represent well oriented planes within the regional stress field. This suggests that stress rotations induced by the main shock for these two intracontinental sequences are unlikely.

In addition, the percentage of well oriented aftershock rupture planes reaches 100% for Colfiorito and 86% for Chi-Chi if we consider a magnitude threshold above  $M_w=3.7$  and  $M_w=5.0$ , respectively. We interpret this as the fact that stress heterogeneities if present are generally localised and can influence only small structures capable of generating small magnitude aftershocks.

© 2007 Elsevier B.V. All rights reserved.

*Keywords:* normal faults; reverse faults; reactivation; aftershocks

## 1. Introduction

Frictional fault reactivation is a well established phenomenon. Geological evidence that faults accumulate kilometres of displacement by repeated movements come from fault-related stratigraphic separations and from the effect produced by large displacement and

high slip-rate faults on the landscape. Considering reactivation from a mechanical point of view, the potential of a fault to undergo slip depends on its orientation within the stress field. Faults well-oriented for reactivation are those where shear stresses are sufficiently high to overcome the frictional resistance, given by the normal stress,  $\sigma_n$ , times the sliding friction coefficient,  $\mu_s$  [1,2].

Frictional fault reactivation is also critical to seismogenesis because the majority of the earthquakes arise mostly from frictional instability on existing faults

\* Corresponding author. Tel.: +39 075 5867182; fax: +39 075 5852603.

E-mail address: [colle@unipg.it](mailto:colle@unipg.it) (C. Collettini).

[3]. Deformation in the intraplate continental crust is characterised, to first order, by coherent stress patterns over large regions (e.g. [4–6]) and this suggests that the major earthquakes nucleating in these areas are controlled by large scale tectonic processes. 2D frictional fault reactivation theory explains well the geometry of moderate to large main shock fault-ruptures nucleating in extensional and compressional intracontinental environments [7,8]. In the two dimensional case, where the strike of the earthquake rupture is assumed to contain the  $\sigma_2$  axis, the dip distribution of the ruptures are consistent with frictional theory predictions and faults possessing a friction coefficient  $\mu_s=0.6$ , at the bottom of the Byerlee's range [7,8]. The prediction of frictional reactivation under Byerlee's friction law is also consistent with in situ stress measurements in deep boreholes [9].

Although frictional fault reactivation theory shows a good correlation with fault–slip analysis [10], dip–slip main shock rupture planes [7,8] and in situ stress measurements [9] the applicability of fault reactivation theory to aftershock sequences has not been fully tested.

Following a major event, aftershocks account for the process of relaxing stress concentration produced by the main shock. In order to explain the physical process controlling earthquake triggering and the time–space evolution of aftershock sequences, several studies have shown correlations with static stress transfer (e.g. [11–14]), stressing rate changes [15,16], poro-elastic effects [17,18], pore fluid diffusion [19–22] or viscoelastic stress transfer (e.g. [23]).

Irrespective of the physical mechanism for aftershock triggering our goal is to test if aftershocks occur on planes prone to fault reactivation within the regional stress field. Departures from this condition might be related to a main shock stress–drop that exceeds the regional stress field, as proposed for the kinematic heterogeneous aftershock sequences of the 1989 ( $M_w=6.9$ ) Loma Prieta earthquake [24], and the 1995 ( $M_w=7.2$ ) Aqaba earthquake [25], or a main shock induced stress rotation that may change the orientation of the stress tensor, as proposed for the Izmit 1999,  $M_w=7.4$  sequence [26].

Since the aftershock ruptures nucleate in the entire seismogenic volume surrounding the main shock and on differently oriented planes that do not necessarily contain the regional  $\sigma_2$  axis, we first introduce a 3D fault reactivation analysis and then compare theoretical predictions with the orientation of the observed aftershock rupture planes for two intracontinental seismic sequences that nucleated in extensional and compressional environments.

## 2. Method

Amonton's law :

$$\tau = \mu_s \sigma'_n \quad (1)$$

governs fault reactivation, where  $\tau$  and  $\sigma'_n$  are, respectively, the shear and effective normal stress (e.g., normal stress,  $\sigma_n$ , minus fluid pressure,  $P_f$ ) acting on the plane of weakness and  $\mu_s$  is the sliding friction coefficient [27]. According to this law, stability is determined by the ratio of shear stress to normal stress acting on the plane of weakness and defined as the slip tendency,  $T_s$  [10,28,29]. Unstable planes are those where

$$T_s = \tau/\sigma'_n > \mu_s. \quad (2)$$

For known values of the principal effective stresses  $\sigma'_1=(\sigma_1-P_f) > \sigma'_2=(\sigma_2-P_f) > \sigma'_3=(\sigma_3-P_f)$  the shear and effective normal stresses acting on a given plane depend on the orientation of the planes [1]:

$$\sigma'_n = \sigma'_1 l^2 + \sigma'_2 m^2 + \sigma'_3 n^2 \quad (3)$$

$$\tau = [(\sigma_1-\sigma_2)^2 l^2 m^2 + (\sigma_2-\sigma_3)^2 m^2 n^2 + (\sigma_3-\sigma_1)^2 l^2 n^2]^{1/2} \quad (4)$$

where  $l$ ,  $m$  and  $n$  are the direction cosines of the plane's normal with respect to the principal stress axes,  $\sigma_1$ ,  $\sigma_2$  and  $\sigma_3$  respectively. Eqs. (3) and (4) define effective normal stress and shear stress for a compressional environment, i.e. horizontal  $\sigma'_1$ : by changing the order of the direction cosines in these equations it is possible to derive effective normal stress and shear stress in extensional and wrench regimes (e.g. [30], p. 785–788). By calculating Eqs. (3) and (4) for all the planes in a 3D space, substituting in Eq. (2) and plotting the results in equal area stereonet we obtain slip tendency stereoplots [10,28,29].

The  $T_s$  stereoplots allow the visualisation of fault reactivation in a 3D space with unstable planes having  $T_s$  higher than the assumed fault friction coefficient.

In a crustal volume with a fixed orientation of the stress field the number of differently oriented planes that reach the condition for frictional reactivation is mainly dependent on the fluid pressure  $P_f$ , the differential stress,  $\sigma_1-\sigma_3$ , the sliding friction coefficient,  $\mu_s$ , and the stress shape ratio  $\phi=(\sigma_2-\sigma_3)/(\sigma_1-\sigma_3)$ . Fig. 1 shows the number of planes susceptible to fault reactivation as a function of increasing fluid pressure, i.e. the pore fluid factor  $\lambda=P_f/\rho g z$ , where  $\rho$  is the crustal density,  $g$  is the

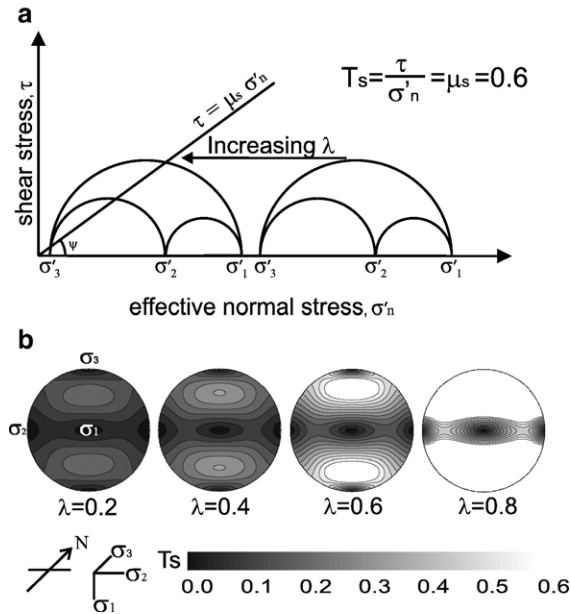


Fig. 1. Influence of fluid pressure on the number of planes prone to fault reactivation i.e. planes possessing  $T_s > 0.6$ . a) Definition of the state of stress in a Mohr diagram where Mohr arbelos represents principal stresses, and the Mohr circles have shape defined by the stress shape ratio  $\phi$ . By increasing the pore fluid factor,  $\lambda$ , the Mohr circle shifts to the left and more and more planes exceed the reactivation condition  $T_s = \tau/\sigma_n > 0.6$ . b) Same phenomenon illustrated by using slip tendency stereoplots for an extensional stress field, vertical  $\sigma_3$  and north-trending  $\sigma_1$ ; poles to planes prone to fault reactivation plot in the white areas.

acceleration due to gravity and  $z$  is the crustal depth. For low values of fluid pressure,  $\lambda = 0.2\text{--}0.4$ , no planes meet the condition for fault reactivation, for  $\lambda = 0.6$  fault reactivation occurs on east–west trending planes dipping in the range  $50^\circ\text{--}60^\circ$ , and for  $\lambda = 0.8$  fault reactivation is possible along all the planes except those trending in the north–south direction. The same influence in the number of planes prone to fault reactivation is observed with increasing differential stress.

However, in a seismogenic volume, both  $P_f$  and  $\sigma_1 - \sigma_3$  are not well-constrained. We overcome this restriction by assuming that the frictional sliding envelope given by Eq. (1) is tangential to the  $\sigma_1\sigma_3$  Mohr circle (Fig. 2). This assumption relates the principal stresses to the equations [10]:

$$\sigma_1 = 1/2k(\csc(\Psi) + 1) \quad (5)$$

$$\sigma_2 = \sigma_1 - k(1 - \phi) \quad (6)$$

$$\sigma_3 = \sigma_1 - k \quad (7)$$

where  $\Psi$  is the angle of sliding friction, with  $\tan\Psi = \tau/\sigma_n$ , and  $k$  is the differential stress. By substituting Eqs. (5)–(7) in Eqs. (3) and (4) and then in Eq. (2), we are able to evaluate slip tendency stereoplot in a mechanical system that is independent of fluid pressure and differential stress, and depends only on the orientation of the stress tensor and stress shape ratio. The variation in the friction coefficient is a second order effect and the Byerlee's values adopted in our analysis are a good approximation for intraplate continental crust [9].

With the tangential condition assumption we do not evaluate the condition for reactivation of a plane of weakness within a given stress field, but rather the slip potential of a fault. In doing this we evaluate the normalised slip tendency,  $NT_s \leq T_s/\max T_s$ , and we define well oriented planes, WOP, for  $0.5 < NT_s \leq 1.0$  and misoriented planes, MOP, for  $0 \leq NT_s \leq 0.5$  (Fig. 2).

In this study we apply this method to two well-documented seismic sequences that occurred in extensional and compressional environments, respectively, the 1997  $M_w = 6.0$  Colfiorito sequence (Central Italy) and the

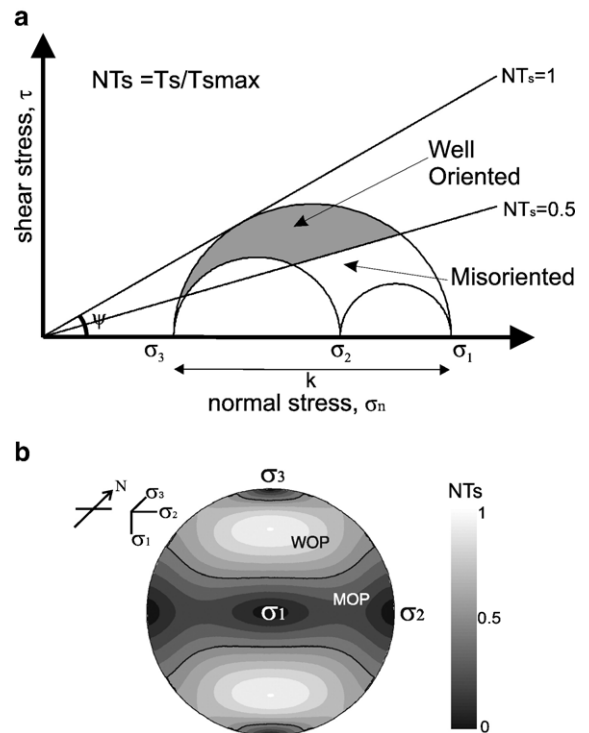


Fig. 2. a) Mohr diagram where the frictional sliding envelope is maintained in the tangential condition to the  $\sigma_1\sigma_3$  Mohr circle following Eqs. (5)–(7) (see text for details).  $\Psi$  is the angle of sliding friction, with  $\tan\Psi = \tau/\sigma_n$ , and  $k$  is the maximum differential stress. b) Slip tendency stereoplot where  $NT_s = T_s/\max T_s$  is the normalised slip tendency. Well oriented planes, WOP, for  $0.5 < NT_s \leq 1.0$  and misoriented planes, MOP, for  $0 \leq NT_s \leq 0.5$ .

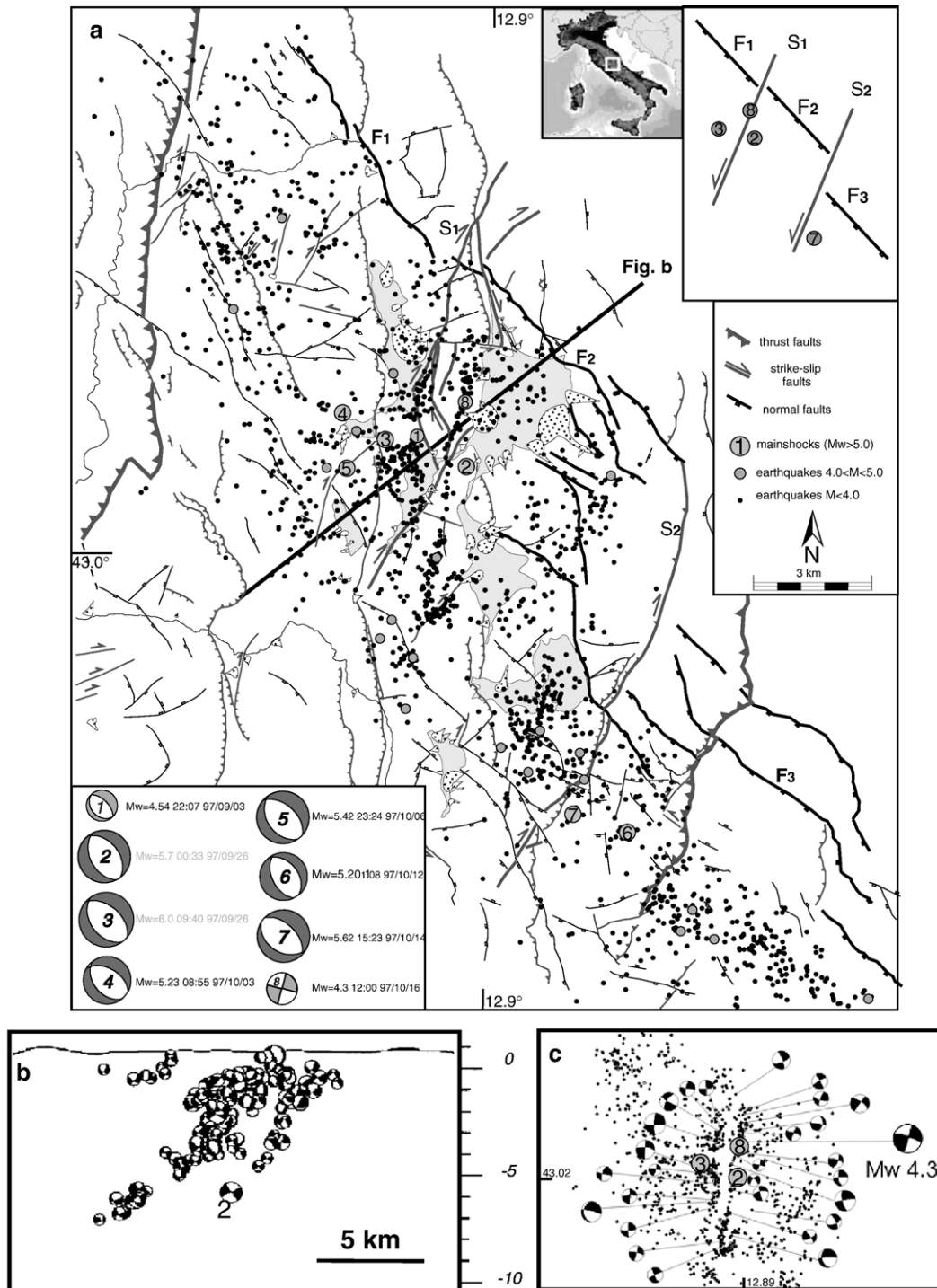


Fig. 3. Geological structures [32,33] and seismicity [31] of the Colfiorito area. (a) Major events nucleate on southwest dipping structures and are characterised by dip-slip kinematics, minor faults are reactivated as left-lateral strike-slip structures. The inset shows a schematic representation of the structures activated during the 1997 sequence, details can be found in [32]. (b) Cross-section showing the southwest dipping ruptures characterised by dip-slip kinematics. (c) Map view showing the details of the north-south trending left-lateral strike-slip fault.

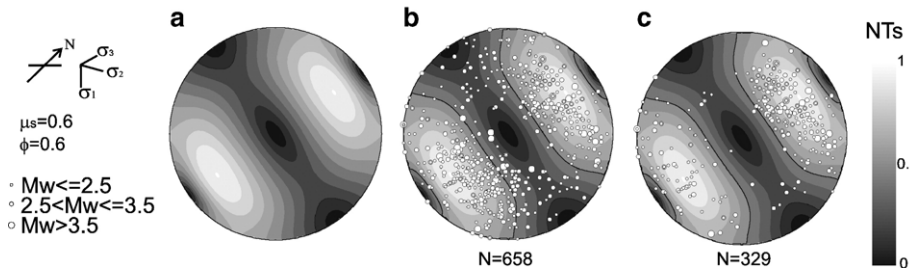


Fig. 4. Slip Tendency Stereoplots for the Colfiorito seismic sequence (see text for an explanation on the adopted stress field parameters). a)  $NT_s$  stereoplot. b)  $NT_s$  stereoplot integrated with all the 658 poles to aftershock rupture planes (white circles) c)  $NT_s$  stereoplot with poles to the 329 positively discriminated aftershock rupture planes. Solid black lines in b) and c) divide the fields of well-oriented and misoriented faults.

1999  $M_w=7.5$  Chi-Chi sequence (Taiwan). We will first reconstruct the slip tendency stereoplots for the two seismic sequences. Then we plot the poles of the aftershock rupture planes in the obtained stereoplots to check if aftershocks nucleate on planes prone to reactivation.

### 3. The 1997 Colfiorito sequence, Central Italy

In September–October 1997, the Colfiorito area (located in the Umbria–Marche Apennines, central Italy) experienced a protracted seismic sequence (Fig. 3) consisting of six extensional main shocks ( $5.0 < M_w < 6.0$  events from 2 to 7) and a subsequent strike–slip event ( $M_w=4.3$ , event 8) that occurred spatially in between the two larger extensional main shocks (event 2 and 3, [31]). The aftershock distribution shows the same geometry and kinematics of the fault system mapped at the surface [32]. In particular, extensional earthquakes occur on southwest dipping normal faults (F1, F2 and F3 in Fig. 3a and b) whilst strike–slip events nucleate on north–south trending left lateral strike–slip faults (Fig. 3c) that reactivate with opposite sense of shear strike–slip structures inherited from the previously developed compressional phase (S1 and S2 in Fig. 3a, [33]). Within the active fault system, normal faults possess displacement up to  $\sim 500$  m [34], that in our judgement was achieved during the last 2 Ma by repeated fault reactivation processes similar to the 1997 seismic sequence (e.g. [32]).

To construct the  $NT_s$  stereoplot we adopt an extensional stress field with a stress shape ratio,  $\phi=0.6$ , as inferred from the inversion of the six main shocks [31]. We adopted a north  $55^\circ$  trending  $\sigma_3$  representing the direction of the extension as inferred from the map of the active stress of the area [35]. This direction is consistent with the  $\sigma_3$  orientation obtained from the inversion of the main shocks and is perpendicular to the strike of the major extensional active faults of the Northern Apennines. We use a

friction coefficient,  $\mu_s=0.6$ , that is a good approximation for active normal faults [8].

With these boundary conditions and following the method described in the previous section, the resulting  $NT_s$  stereoplot are reported in Fig. 4. In these stereoplots we plot, as poles, the aftershock rupture planes ( $2.5 < M_L < 6.0$ ) obtained from the focal mechanisms

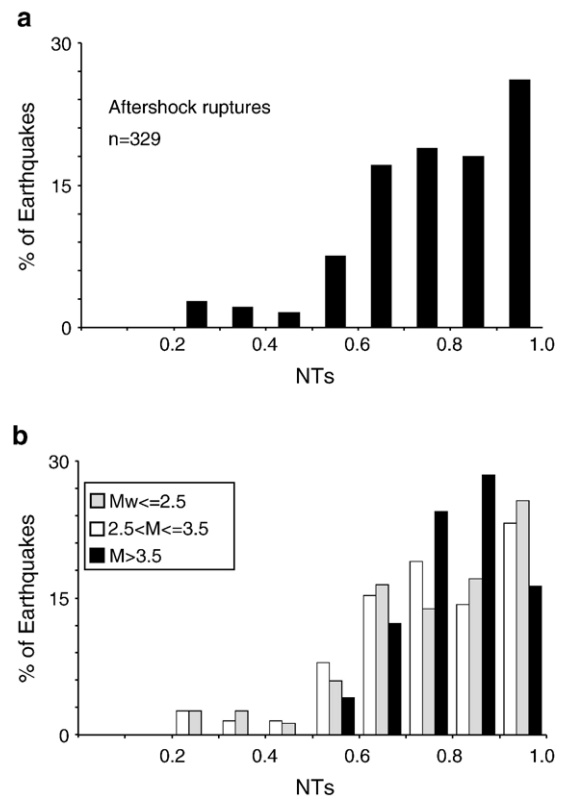


Fig. 5. Slip tendency analysis for the Colfiorito positively discriminated aftershock rupture planes. a)  $NT_s$  values vs. per cent of earthquakes showing a clear increase in the number of earthquakes with increasing  $NT_s$ . b)  $NT_s$  values vs. per cent of earthquakes within a magnitude range: it is worth noting that no earthquakes with  $M > 3.5$  are in the field of misoriented faults, i.e.  $NT_s < 0.5$ .

[31]: Fig. 4b shows the 658 aftershock rupture planes whilst Fig. 4c shows the positively discriminated ruptures. The focal mechanisms of the sequence can be divided into two main groups. The first group is represented by extensional earthquakes with location along the southwest dipping normal faults and focal mechanisms similar to the main shocks: both planes north-west trending and characterised by opposite dips (events 2–7 in Fig. 3a and b). The second group is represented by strike–slip focal mechanisms located along the north–south trending structures and possessing one north–south trending plane with left-lateral kinematics and one east–west trending plane with right-lateral kinematics: these aftershocks possess focal mechanisms similar to the major strike–slip event (event 8 in Fig. 3a and c). To positively discriminate the focal mechanisms, for the first group we selected south-west dipping planes and for the second group we selected north–south trending ruptures (Fig. 3). In the ambiguous cases we selected the nodal plane with the geometry closer to either north-west or north–south trending direction.

From the fault reactivation analysis results that 72% of all the aftershock rupture planes occur on planes prone to fault reactivation within the regional stress field ( $NT_s < 0.5$  in Fig. 4b) and this percentage reaches the 89% if we consider the positively discriminated ruptures (Fig. 4c). The 17% increase of well explained ruptures when we consider positively discriminated nodal planes (Fig. 4c) is the result of: a) the presence of focal mechanisms with one south-west dipping plane and the other plane trending east–west. In this case adopting our selection criteria we choose the south-west dipping plane as the true rupture plane and the negatively discriminated east–west trending plane is misoriented and results in a low  $T_s$ ; b) strike–slip events with one north–south and another  $\sim$ east–west trending plane. Again, following our selection criteria we selected the north–south trending plane as the true rupture plane and the negatively discriminated  $\sim$ east–west trending rupture results in low  $T_s$ . Finally, it is worth noting that in doing these calculations we considered the thrust–slip solutions as ruptures occurring in the field of severely misoriented faults, and therefore in the 11% of the ruptures not explained by our analysis, since they are in disagreement with the applied extensional stress field.

Within the positively discriminated aftershock rupture planes,  $\sim 30\%$  of them occur on planes where  $NT_s$  is in the range 0.9–1.0, whilst the majority of the ruptures,  $\sim 50\%$ , lies in the range  $0.6 < NT_s < 0.9$  (Fig. 5a). This suggests that the majority of aftershocks nucleate as reactivation of geological structures, in particular gently

dipping normal faults (dip  $\sim 40^\circ$ ) and steeply dipping strike–slip or transtensional structures, which are well oriented within the regional stress field but not optimally oriented. In addition, the few earthquakes inconsistent with the reactivation theory, i.e. those ruptures occurring on planes where  $NT_s < 0.5$ , possess small magnitudes,  $M < 3.5$ , whilst 100% of the  $M > 3.5$  earthquakes show  $NT_s > 0.5$  (Fig. 5b). Since the Colfiorito aftershock sequence seems to be fluid-driven [21,22], localised fluid overpressures could have triggered ruptures on less favourably oriented faults. Alternatively the small ruptures nucleating on misoriented planes would be the result of local stress heterogeneities induced by the main shock.

Our analysis based on Eq. (1) considers reactivation from a mechanical viewpoint. To test the reliability of the imposed stress field with the kinematics of the activated structures, we performed a fault kinematics control on positively discriminated ruptures by plotting the aftershock rupture planes as a function of the rake angle (e.g. [36]): reverse slip,  $45^\circ$  to  $135^\circ$ ; left-lateral strike slip  $-45^\circ$  to  $45^\circ$ ; right-lateral strike slip  $-135^\circ$  to  $-180^\circ$  and  $135^\circ$  to  $180^\circ$ ; normal slip  $-45^\circ$  to  $-135^\circ$ . In agreement with the orientation of the seismogenic structures within the regional stress field we observe that northwest–southeast trending planes are characterised by dip–slip movements whilst north–south trending structures possess transtensional left-lateral strike–slip kinematics (Fig. 6).

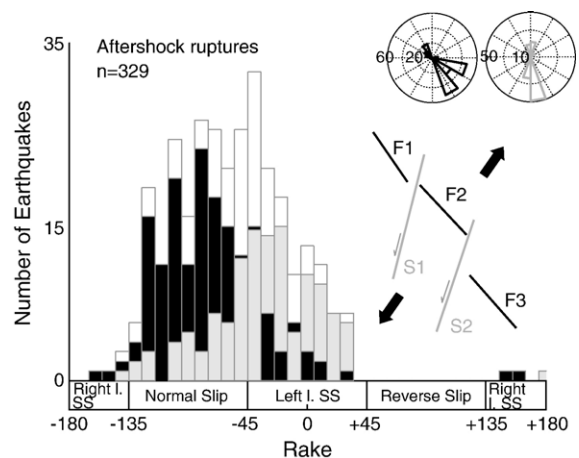


Fig. 6. Kinematic analysis of Colfiorito positively discriminated aftershock rupture planes. In agreement with the regional NE–SW trending extension (black arrows) SW dipping planes (black bins and rose diagrams) show predominant dip–slip and transtensive movements whilst north–south trending ruptures are characterised by left-lateral to transtensive kinematics (grey bins and rose diagrams). The white bins represent the sum of black and grey bins.

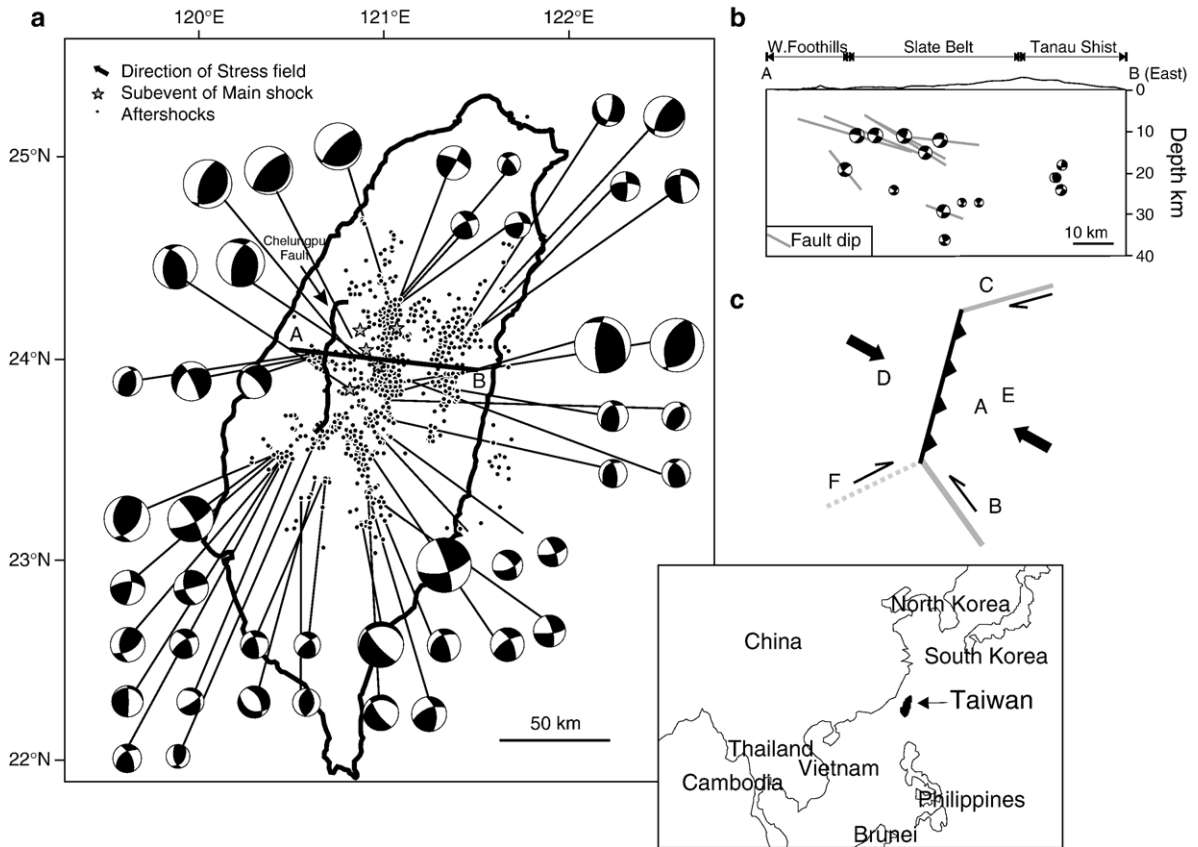


Fig. 7. Chi-Chi 1999 seismic sequence (Taiwan) and aftershocks focal mechanisms (after [37]). a) Map showing epicentres of the Chi-Chi sequence and fault plane solutions. b) Cross-section through the Chelungpu fault: the aftershock distribution highlights two east-dipping thrusts active at different crustal levels [37]. c) The 6 groups of focal mechanisms with the associated structures identified by [37].

The analysis applied to the Colfiorito aftershock sequence point to a strong mechanical and structural control on the aftershock rupture planes. Although the area is characterised by the presence of faults with different orientation resulting from three different tectonic phases, Jurassic syn-sedimentary extension, Upper Miocene Lower Pliocene compression and Upper Pliocene Quaternary extension, the rupture planes

nucleate predominantly on geological structures that are well-oriented,  $NT_s > 0.5$ , within the regional stress field.

#### 4. The 1999 Chi-Chi seismic sequence, Taiwan

The Chi-Chi seismic sequence occurred along the western portion of the Taiwan orogen. The  $M_w = 7.5$

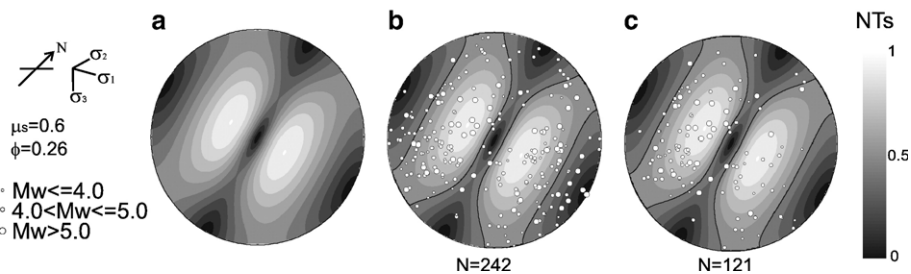


Fig. 8. Slip Tendency stereoplots for the Chi-Chi seismic sequence (see text for an explanations of the adopted boundary condition). a)  $NT_s$  stereoplots. b)  $NT_s$  stereoplots integrated with all the 242 poles to aftershock rupture planes (white circles) c)  $NT_s$  stereoplots with the poles to the 121 positively discriminated aftershock rupture planes. Solid black lines in b) and c) divide the fields of well-oriented and misoriented faults.

main shock nucleated on the Chelungpu fault that showed a surface rupture of  $\sim 80$  km. The kinematics of the main event shows a thrust fault following a plane dipping  $25^\circ$  eastward down to a depth of 15 km [37]. The main shock was followed by an intense aftershock sequence recorded by the Central Weather Bureau Seismographic Network (CWBSN), and distributed over central Taiwan (Fig. 7). Following [37] six groups of aftershocks, A–F in Fig. 7c, can be identified. The aftershock sequence, is dominated by reverse slip and strike–slip focal mechanisms. The thrust slip events (Fig. 7) are associated with the Chelungpu fault and to another parallel thrust zone about 15 km directly beneath the main rupture zone and forming a deep seismogenic rupture at depths of about 25–30 km (group A, after [37]). Strike–slip focal mechanisms nucleated near the ends of the Chelungpu fault and, although these events cannot be related to mapped structures, earthquake alignments and focal mechanisms appear consistent with east–west right-lateral and northwest–southeast trending left-lateral shear zones located at the northern, group C, and southern portion, group B, of the Chelungpu fault. The aftershocks of group F seem to activate a conjugate system of group B whilst group D nucleated on the footwall of the Chelungpu fault and appears to be not directly linked to the activated major structures. The inversion of the aftershocks of the 1999 seismic sequence is consistent with the patterns of long-term stress field inferred from geological evidence [38], with the exception of the increase in strike–slip mechanisms to the southeast of the Chelungpu fault, the aftershock distribution and kinematics is similar before and after the Chi-Chi earthquake [14]. These two observations suggest that the process of active mountain building in Taiwan, operates primarily by repeated fault reactivation along the same structures.

To test if the aftershocks of the Chi-Chi sequence occurred on planes prone to fault reactivation, we construct a  $NT_s$  stereoplots for a compressional stress field. We adopted a friction coefficient,  $\mu_s=0.6$ , [7], a stress shape ratio,  $\phi=0.26$ , [38], and a north  $120^\circ$  trending  $\sigma_1$ . This is in agreement with both plate motions, the Philippine sea plate and Eurasia plate in particular (e.g. [39]), and active stress of the area [38,40].

Using these boundary conditions, the  $NT_s$  stereoplots for the Chi-Chi seismic sequence is shown in Fig. 8a. In these stereoplots we plot, as poles, the aftershock rupture planes ( $3.6 < M_w < 7.5$ ) obtained from the focal mechanisms [38]. Fig. 8b shows the 242 aftershock rupture planes whilst Fig. 8c shows the 121 positively

discriminated ruptures. To positively discriminate the rupture planes, we selected ruptures consistent with the geometry of the activated structure that is represented by a north–south trending east-dipping fault that terminates to the north in a  $\sim$ east–west trending fault (group C) and to the south in a north–west trending structure. Therefore we selected north–south trending, predominantly east-

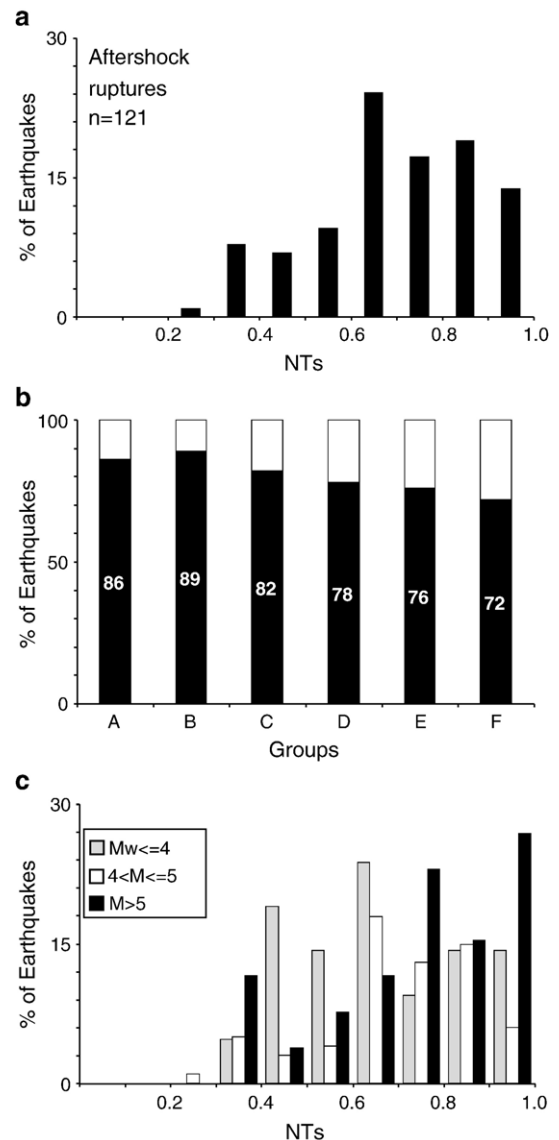


Fig. 9. Slip tendency analysis of the Chi-Chi positively discriminated aftershock rupture planes. a)  $NT_s$  values vs. number of earthquakes showing a great number of ruptures in the field  $0.6 < NT_s < 0.9$ . b) Percentage of planes possessing  $NT_s > 0.5$  divided by group: best explained ruptures belong to groups A, B and C that are the groups closely related to the main rupture. c)  $NT_s$  values vs. per cent of earthquakes showing that the percentage of well oriented planes increases with increasing magnitude.

dipping planes for groups A, D and E, east–west trending planes for groups C and F and northwest–southeast trending planes for group B.

From the fault reactivation analysis, 74% of all the aftershock rupture planes occur on planes prone to fault reactivation within the regional stress field ( $NT_s > 0.5$  in Fig. 8b). This percentage reaches 81% if we consider the positively discriminated ruptures (Fig. 8c). In this case as well, we have considered the normal-slip solutions as ruptures occurring in the field of severely misoriented faults since they are in disagreement with the applied compressional stress field.

For the Chi-Chi aftershock sequence the majority of rupture planes,  $\sim 30\%$ , fall in the range  $0.6 < NT_s < 0.7$

and 65% of the ruptures lies in the field  $0.6 < NT_s < 0.9$  with only  $\sim 15\%$  of planes where  $NT_s$  is in the range  $0.9–1.0$  (Fig. 9a). This occurs because of the abundance of the steeply dipping strike–slip solutions that are not optimally oriented in the regional compressional stress field. The  $NT_s$  analysis performed for each subsets of data (Fig. 9b) shows that the best explained ruptures belong to groups A, B and C that are the groups spatially closely related to the main rupture of the sequence (Fig. 9b). The remaining groups show a lower number of consistent planes with a percentage of 78%, 76% and 72% for groups D, E and F respectively. Within these groups some ruptures with  $NT_s < 0.5$  could be the result of local variation in the state of stress (e.g. [38]).

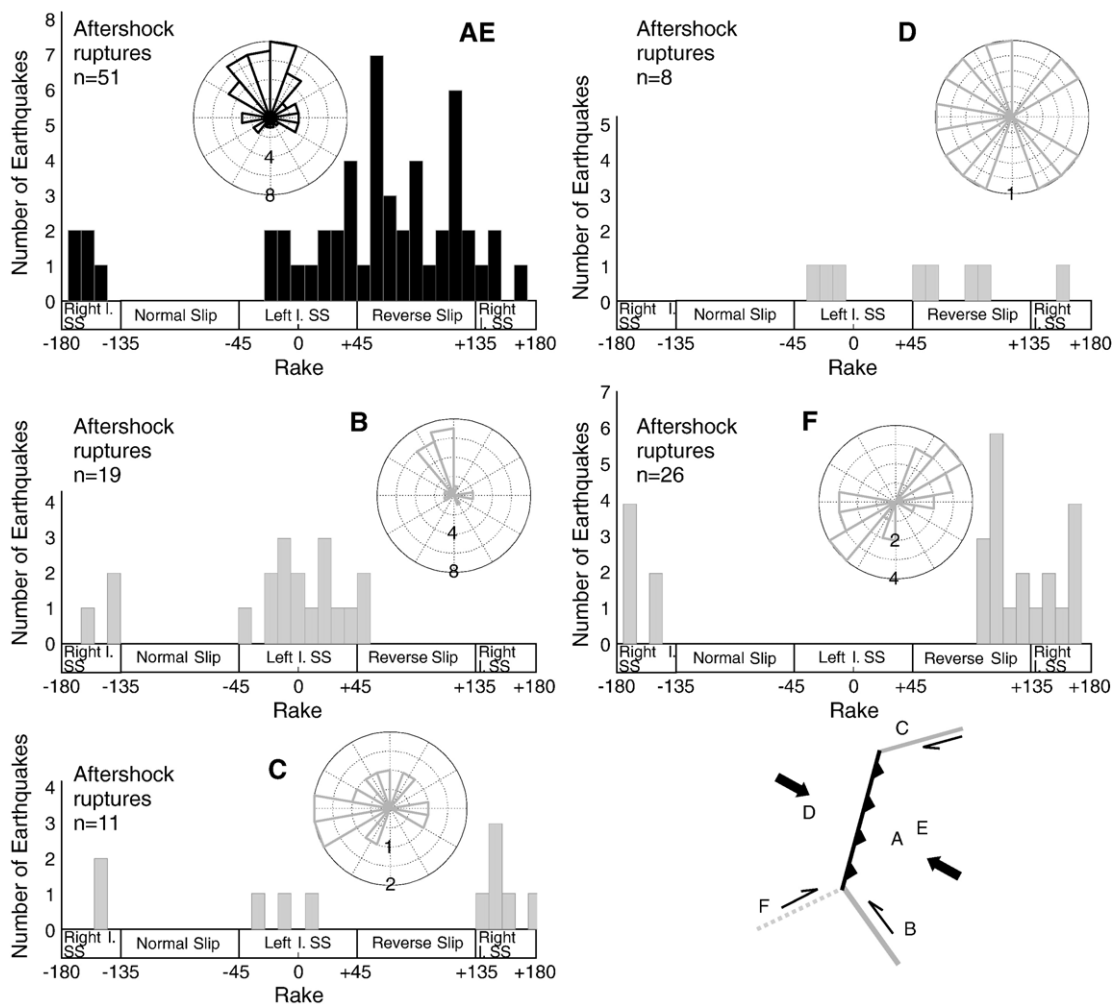


Fig. 10. Kinematic analysis of Chi-Chi positively discriminated aftershock rupture planes. Ruptures occur on north–south trending planes with predominant reverse-slip kinematics (groups A and E), northeast trending planes with left-lateral strike–slip ruptures (group B), east-southeast trending ruptures with right-lateral strike–slip kinematics (group C), northwest trending ruptures with right-lateral strike–slip kinematics (group F). The only group of aftershocks not correlated with the geometry of the structures within the regional stress field is group D characterised by earthquakes with randomly oriented planes possessing reverse and strike–slip kinematics.

To analyse the  $NT_s$  values as a function of the magnitude (Fig. 9c), we have divided the dataset in three groups:  $M < 4.0$ ,  $4.0 \leq M < 5.0$  and  $M \geq 5.0$ . We observe that the percentage of the ruptures with  $NT_s > 0.5$  increases with increasing magnitude: in particular we have the 79%, 81% and 86% of events with  $NT_s > 0.5$  for magnitudes in the ranges  $M < 4.0$ ,  $4.0 \leq M < 5.0$  and  $M \geq 5.0$  respectively (Fig. 9c). We noted that between the aftershocks with  $M \geq 5.0$  two of the ruptures ( $\sim 50\%$ ) that fall in the field of misoriented faults nucleated in the same day of the main shock, suggesting a possible stress rotation produced by the main shock.

Finally, we performed a kinematics control by plotting the aftershock rupture planes as a function of both group and rake angle (Fig. 10). Within groups A and E ruptures occur on north–south trending planes with predominant reverse-slip kinematics, group B results in north-east trending left-lateral strike–slip ruptures, group C is characterised by east-southeast trending right-lateral strike–slip ruptures, group F contains north-west trending right-lateral strike–slip structures and group D is characterised by strike–slip and reverse ruptures with different orientations. Except for group D, that however is made of only 8 ruptures, all the groups are characterised by aftershock kinematics consistent with the orientation of the faults within the regional stress field.

## 5. Discussion and conclusions

We performed a 3D fault–slip analysis based on the orientation of the regional stress field to determine whether the fraction of aftershock rupture planes predicted by frictional reactivation theory is greater than the fraction of random events ( $\sim 50\%$ ), which would appear to be consistent by chance. In particular, 89% of 329 and 81% of 121 positively discriminated events for the Colfiorito and Chi-Chi sequences respectively are well explained by fault reactivation processes within the prevailing regional stress field.

The nucleation of the aftershock ruptures on well-oriented planes for fault reactivation in the regional stress field, suggests that aftershock ruptures are mainly loaded to failure by tectonic stresses and the main shock induced stress perturbations, e.g. static stress changes [11–14,41] or increase in fluid pressure (e.g. [21]), would trigger aftershocks on planes already close to failure.

In addition, the positive correlation of the orientation of the aftershock ruptures with the regional stress field for the two studied sequences suggests that the static stress drop induced by the main shocks — usually in the

range of 1–10 MPa [42,43] is not enough to totally release the tectonic stress level (e.g. [44]). Therefore, following a major event, the orientation of the aftershock rupture planes is still governed by the regional stress field. In other words the stress level of the seismogenic volumes activated during the two intracontinental seismic sequences, was well above the stress changes induced by the main shocks. This is also confirmed by stress level measurements in deep intraplate boreholes showing an increase of the differential stress with depth and values greater than 100 MPa at depths greater than 5 km [9].

For the two studied sequences the percentage of well oriented aftershock rupture planes significantly increases if we consider only events above a certain magnitude threshold. For the Colfiorito sequence the percentage of well oriented rupture planes reaches  $\sim 100\%$ , if we consider an  $M_L = 3.7$  threshold and for the Chi-Chi sequence the percentage increase from 79% to 81% up to 86% if we consider magnitude intervals in the range  $M < 4.0$ ,  $4.0 \leq M < 5.0$  and  $M \geq 5.0$  respectively. We interpret this as the fact that in a strong crust stress rotations induced by the main shock are unlikely, or if present, are extremely localised and can influence only small structures capable of generating small magnitude aftershocks. Similar conclusions have been proposed for the Landers 1992,  $M_w = 7.3$  seismic sequence by the inversion of the focal mechanisms ([44] but see also [45]) and by the correspondence of aftershock rupture planes with mapped structures [46].

Within the aftershock rupture planes consistent with reactivation theory, a small percentage nucleate on planes optimally oriented for failure ( $NT_s$  close to 1.0) in the prevailing regional stress field, 30% for Colfiorito and 15% for Chi-Chi. A great number of ruptures occur on planes prone to reactivation but not optimally oriented, 50% of the Colfiorito aftershocks and 65% of Chi-Chi events fall in the range  $0.6 \leq NT_s < 0.9$ . This is because in a crustal volume where optimally oriented faults are lacking or not abundant, the majority of aftershocks occur as reactivation of geological structures prone to fault reactivation in the prevailing stress field. This suggests that the routine assumption in Coulomb failure stress studies, that aftershocks occur on optimally oriented faults (but see also [41] and [46]), may sometimes be inconsistent with the real orientation of the aftershock rupture planes. In our view the two studied seismic sequences provide an insight into the long-term deformation process that is achieved by repeated reactivation of geological structures and that allows crustal extension in the Northern Apennines of Italy and mountain building on the Taiwan orogen.

Finally, since aftershocks represent a serious hazard because they nucleate in areas already weakened by the main shock, our findings suggest that in seismically active areas a detailed catalogue of crustal scale structures well oriented within the regional stress field would help in improving real time aftershock hazard estimates.

## Acknowledgments

This research was supported by COFIN05 C. Collettini grant and it has benefited greatly from continuous and stimulating discussions with L. Chiaraluce and N. De Paola and helpful comments from S. Bagh, R. Caputo and G. Minelli. A. Antonioli, M.R. Barchi and S. Miller reviewed an earlier version of the manuscript. We thank D. Healy and an anonymous referee for constructing reviews.

## References

- [1] J.G. Jaeger, G.W. Cook, *Fundamentals of Rock Mechanism*, third ed., Chapman and Hall, London, 1979 585 pp.
- [2] R.H. Sibson, A note on fault reactivation, *J. Struct. Geol.* 7 (1985) 751–754.
- [3] C.H. Scholz, Earthquakes and friction laws, *Nature* 391 (1998) 37–42.
- [4] M.L. Zoback, M.D. Zoback, First and second order patterns of tectonic stress: the World Stress Map Project, *J. Geophys. Res.* 97 (1992) 11703–11728.
- [5] M.D. Zoback, State of stress in the Earth's lithosphere, *Int. Handb. Earthq. Eng. Eng. Seismol.* 81A (2002) 559–568.
- [6] <http://www.world-stress-map.org>.
- [7] R.H. Sibson, G. Xie, Dip range for intracontinental reverse fault ruptures: truth not stranger than friction? *Bull. Seismol. Soc. Am.* 88 (1998) 1014–1022.
- [8] C. Collettini, R.H. Sibson, Normal fault, normal friction? *Geology* 29 (2001) 927–930.
- [9] J. Townend, M.D. Zoback, How faulting keeps the crust strong, *Geology* 28 (2000) 399–402.
- [10] R.J. Lisle, D.C. Srivastava, Test of the frictional reactivation theory for faults and validity of fault–slip analysis, *Geology* 32 (7) (2004) 569–572.
- [11] R.A. Harris, Introduction to special section: stress triggers, stress shadows, and implications for seismic hazard, *J. Geophys. Res.* 103 (1998) 24,347–24,358.
- [12] R.S. Stein, The role of stress transfer in earthquake occurrence, *Nature* 402 (1999) 605–609.
- [13] G.C.P. King, M. Cocco, Fault interaction by elastic stress changes: new clues from earthquake sequences, *Adv. Geophys.* 44 (2000) 1–38.
- [14] K.F. Ma, C.H. Chan, R.S. Stein, Response of seismicity to Coulomb stress triggers, shadows of the 1999 M<sub>w</sub>=7.6 Chi-Chi, Taiwan, earthquake, *J. Geophys. Res.* 110 (2005) B05S19, doi:10.1029/2004JB003389.
- [15] J. Dieterich, A constitutive law for rate of earthquake production and its application to earthquake clustering, *J. Geophys. Res.* 99 (B2) (1994) 2601–2618.
- [16] S. Toda, R. Stein, T. Saglya, Evidence from the AD 2000 Izu islands earthquake swarm that stressing rate governs seismicity, *Nature* 419 (2002) 58–61.
- [17] A. Nur, J.R. Booker, Aftershocks caused by pore fluid flow? *Science* 175 (1972) 885–887.
- [18] W. Bosl, A. Nur, Aftershocks and pore fluid diffusion following the 1992 Landers earthquake, *J. Geophys. Res.* 107 (B12) (2002) 1–12.
- [19] J. Noir, E. Jacques, S. Bèkri, P.M. Adler, G.C.P. King, Fluid flow triggered migration of events in the 1989 Dobi earthquake sequence of Central Afar, *Geophys. Res. Lett.* 24 (1997) 2335–2338.
- [20] S.A. Shapiro, R. Patzig, E. Rothert, J. Rindshwentne, Triggering of seismicity by pore-pressure perturbations: permeability-related signature of the phenomenon, *Pure Appl. Geophys.* 160 (2003) 1051–1066.
- [21] S.A. Miller, C. Collettini, L. Chiaraluce, M. Cocco, M.R. Barchi, J.P.K. Boris, Aftershocks driver by high pressure CO<sub>2</sub> source at depth, *Nature* 427 (2004) 724–727.
- [22] A. Antonioli, D. Piccinini, L. Chiaraluce, M. Cocco, Fluid flow and seismicity pattern: evidence from the 1997 Umbria–Marche (central Italy) seismic sequence, *Geophys. Res. Lett.* 32 (2005) L10311, doi:10.1029/2004GL022256.
- [23] A.M. Freed, J. Lin, Delayed triggering of the Hector Mine earthquake by viscoelastic stress transfer, *Nature* (2001) 180–183.
- [24] A.J. Michael, Energy constraints of kinematics models of oblique faulting; Loma Prieta versus Parkfield–Coalinga, *Geophys. Res. Lett.* 17 (1990) 1453–1456.
- [25] A. Hofstetter, H.K. Thio, G. Shamir, Source mechanism of the 22/11/95 Gulf of Aqaba earthquake and its aftershock sequence, *J. Seismol.* 7 (2003) 99–114.
- [26] M. Bohnhoff, H. Gresser, G. Dresen, Strain partitioning and stress rotation at the North Anatolian fault zone from aftershock focal mechanisms of the 1999 Izmit Mw=7.4 earthquake, *Geophys. J. Int.* 166 (1) (2006) 373.
- [27] J.D. Byerlee, Friction of rocks, *Pure Appl. Geophys.* 116 (1978) 615–626.
- [28] A. Morris, A. Ferril, D.B. Henderson, Slip tendency analysis and fault reactivation, *Geology* 24 (3) (1996) 275–278.
- [29] J.E. Streit, R.R. Hillis, Estimating fault stability and sustainable fluid pressures for underground storage of CO<sub>2</sub> in porous rock, *Energy* 29 (2004) 1445–1456.
- [30] J.G. Ramsay, R.J. Lisle. The techniques of modern structural geology. Volume 3: Applications of continuum mechanics in structural geology, Academic Press, 2000, pp. 701–1061.
- [31] L. Chiaraluce, W.L. Ellsworth, C. Chiarabba, M. Cocco, Imaging the complexity of an active normal fault system: the Colfiorito (central Italy) case study, *J. Geophys. Res.* 108 (B6) (2003) 2294.
- [32] L. Chiaraluce, M.R. Barchi, C. Collettini, F. Mirabella, S. Pucci, Connecting seismically active normal faults with Quaternary geological structures in a complex extensional environment: the Colfiorito 1997 case history (northern Apennines, Italy), *Tectonics* 24 (2005) TC 1002.
- [33] C. Collettini, L. Chiaraluce, S. Pucci, M.R. Barchi, M. Cocco, Looking at fault reactivation matching structural geology and seismology, *J. Struct. Geol.* 5 (2005) 937–942.
- [34] F. Mirabella, V. Boccali, M.R. Barchi, Segmentation interaction of normal faults within the Colfiorito fault system (Central Italy), *Spec. Publ. - Geol. Soc. Lond.* 243 (2005) 25–36.
- [35] P. Montone, M.T. Mariucci, S. Pondrelli, A. Amato, An improved stress map for Italy and surrounding regions (central

- Mediterranean), *J. Geophys. Res.* 109 (2004) B10410, doi:10.1029/2003JB002703.
- [36] K. Aki, P.G. Richards, *Quantitative Seismology*, second ed. University Science Books, 2002.
- [37] H. Kao, W.P. Chen, The Chi-Chi earthquake sequence: active, out-of sequence thrust faulting in Taiwan, *Science* 288 (2000) 2346–2349.
- [38] H. Kao, J. Angelier, Stress tensor for the Chi Chi Earthquakes sequence and its implication on regional collision, *Bull. Seismol. Soc. Am.* 91 (2001) 1028–1040.
- [39] T. Seno, S. Stein, A.E. Gripp, A model for the motion of the Philippine Sea plate consistent with NUVEL-1 and geological data, *J. Geophys. Res.* 98 (1993) 17941–17948.
- [40] J. Angelier, E. Barrier, H.T. Chu, Plate collision and paleostress trajectories in a fold–thrust belt: the Foothills of Taiwan, *Tectonophysics* 125 (1986) 161–178.
- [41] C. Nostro, L. Chiaraluce, M. Cocco, D. Baumont, O. Scotti, Coulomb stress changes caused by repeated normal faulting earthquakes during the 1997 Umbria–Marche (central Italy) seismic sequence, *J. Geophys. Res.* 110 (2005) B05S20, doi:10.1029/2004JB003386.
- [42] T.C. Hankcs, Earthquake stress drops, ambient tectonic stresses and stresses that drive plate motion, *Pure Appl. Geophys.* 115 (1977) 441–458.
- [43] H. Kanamori, T.H. Heaton, Microscopic and macroscopic physics of earthquakes, in: J.B. Rundle, D.L. Turcotte, W. Klein (Eds.), *AGU Monograph Series*, “Physics of Earthquakes”, 2000, pp. 147–163.
- [44] J. Townend, M.D. Zoback, Implications of earthquake focal mechanisms for the frictional strength of the San Andreas fault system, in: R.E. Holdsworth, R.A. Strachan, J. Macloughlin, R.J. Knipe (Eds.), *The Nature and Tectonic Significance of Fault Zone Weakening*, Special Publication of the Geological Society of London, vol. 186, 2001, pp. 13–21.
- [45] J.L. Hardebeck, E. Hauksson, Role of fluids in faulting inferred from stress field signatures, *Science* 285 (1999) 236–239.
- [46] J. McCloskey, S.S. Nalbant, S. Steacy, C. Nostro, O. Scotti, D. Baumont, Structural constraints on the spatial distribution of aftershocks, *Geophys. Res. Lett.* 30 (12) (2003) 1610, doi:10.1029/2003GL017225.